Comparison of particle production in quark and gluon fragmentation at $\sqrt{s} \sim 10$ GeV

R. A. Briere,[1] T. Ferguson,[1] G. Tatishvili,[1] H. Vogel,[1] M. E. Watkins,[1] J. L. Rosner,[2] N. E. Adam,[3] J. P. Alexander,[3] D. G. Cassel,[3] J. E. Duboscq,[3] R. Ehrlich,[3] L. Fields,[3] R. S. Galik,[3] L. Gibbons,[3] R. Gray,[3] S. W. Gray,[3] D. L. Hartill,[3] B. K. Heltsley,[3] D. Hertz,[3] C. D. Jones,[3] J. Kandaswamy,[3] D. L. Kreinick,[3] V. E. Kuznetsov,[3] H. Mahlke-Krüger,[3] P. U. E. Onyisi,[3] J. R. Patterson,[3] D. Peterson,[3] J. Pivarski,[3] D. Riley,[3] A. Ryd,[3] A. J. Sadoff,[3] H. Schwarthoff,[3] X. Shi,[3] S. Stroiney,[3] W. M. Sun,[3] T. Wilksen,[3] M. Weinberger,[3] S. B. Athar,[4] R. Patel,[4] V. Potlia,[4] J. Yelton,[4] P. Rubin,[5] C. Cawlfield,[6] B. I. Eisenstein,[6] I. Karliner,[6] D. Kim,[6] N. Lowrey,[6] P. Naik,[6] M. Selen,[6] E. J. White,[6] J. Wiss,[6] R. E. Mitchell,[7] M. R. Shepherd,[7] D. Besson,[8] H. K. Swift,[8,*] T. K. Pedlar,[9] D. Cronin-Hennessy,[10] K. Y. Gao,[10] J. Hietala,[10] Y. Kubota,[10] T. Klein,[10] B. W. Lang,[10] R. Poling,[10] A. W. Scott,[10] A. Smith,[10] P. Zweber,[10] S. Dobbs,[11] Z. Metreveli,[11] K. K. Seth,[11] A. Tomaradze,[11] J. Ernst,[12] K. M. Ecklund,[13] H. Severini,[14] W. Love,[15] V. Savinov,[15] O. Aquines,[16] Z. Li,[16] A. Lopez,[16] S. Mehrabyan,[16] H. Mendez,[16] J. Ramirez,[16] G. S. Huang,[17] D. H. Miller,[17] V. Pavlunin,[17] B. Sanghi,[17] I. P. J. Shipsey,[17] B. Xin,[17] G. S. Adams,[18] M. Anderson,[18] J. P. Cummings,[18] I. Danko,[18] D. Hu,[18] B. Moziak,[18] J. Napolitano,[18] Q. He,[19] J. Insler,[19] H. Muramatsu,[19] C. S. Park,[19] E. H. Thorndike,[19] F. Yang,[19] T. E. Coan,[20] Y. S. Gao,[20] M. Artuso,[21] S. Blusk,[21] J. Butt,[21] J. Li,[21] N. Menaa,[21] G. C. Moneti,[21] R. Mountain,[21] S. Nisar,[21] K. Randrianarivony,[21] R. Sia,[21] T. Skwarnicki,[21] S. Stone,[21] J. C. Wang,[21] K. Zhang,[21] G. Bonvicini,[22] D. Cinabro,[22] M. Dubrovin,[22] A. Lincoln,[22] D. M. Asner,[23] and K. W. Edwards[23]

(CLEO Collaboration)

[1]*Carnegie Mellon University, Pittsburgh, Pennsylvania 15213, USA*
[2]*Enrico Fermi Institute, University of Chicago, Chicago, Illinois 60637, USA*
[3]*Cornell University, Ithaca, New York 14853, USA*
[4]*University of Florida, Gainesville, Florida 32611, USA*
[5]*George Mason University, Fairfax, Virginia 22030, USA*
[6]*University of Illinois, Urbana-Champaign, Illinois 61801, USA*
[7]*Indiana University, Bloomington, Indiana 47405, USA*
[8]*University of Kansas, Lawrence, Kansas 66045, USA*
[9]*Luther College, Decorah, Iowa 52101, USA*
[10]*University of Minnesota, Minneapolis, Minnesota 55455, USA*
[11]*Northwestern University, Evanston, Illinois 60208, USA*
[12]*State University of New York at Albany, Albany, New York 12222, USA*
[13]*State University of New York at Buffalo, Buffalo, New York 14260, USA*
[14]*University of Oklahoma, Norman, Oklahoma 73019, USA*
[15]*University of Pittsburgh, Pittsburgh, Pennsylvania 15260, USA*
[16]*University of Puerto Rico, Mayaguez, Puerto Rico 00681*
[17]*Purdue University, West Lafayette, Indiana 47907, USA*
[18]*Rensselaer Polytechnic Institute, Troy, New York 12180, USA*
[19]*University of Rochester, Rochester, New York 14627, USA*
[20]*Southern Methodist University, Dallas, Texas 75275, USA*
[21]*Syracuse University, Syracuse, New York 13244, USA*
[22]*Wayne State University, Detroit, Michigan 48202, USA*
[23]*Carleton University, Ottawa, Ontario, Canada K1S 5B6*
(Received 19 April 2007; published 27 July 2007)

Using $e^+e^- \to$ hadrons data collected with the CLEO-III detector at the Cornell Electron Storage Ring, we study the inclusive production of baryons/antibaryons (p, Λ) and mesons (ϕ and $f_2(1270)$) in gluon-fragmentation and quark-fragmentation processes. We first corroborate previous per-event total particle yields in $\Upsilon(1S) \to ggg$ compared with nearby continuum ($e^+e^- \to q\bar{q}$) indicating greater ($\sim \times 2$) per-event yields of baryons in 3-gluon fragmentation. We find similar results when we extend that comparison to include the $\Upsilon(2S)$ and $\Upsilon(3S)$ resonances. With higher statistics, we now also probe the momentum dependence of these per-event particle yields. Next, we compare particle production in the photon-tagged process $\Upsilon(1S) \to gg\gamma$ with that in $e^+e^- \to q\bar{q}\gamma$ events, to allow comparison of two-parton with three-parton particle-specific fragmentation. For each particle, we determine the "enhancement" ratio, defined as the ratio of particle yields per gluon-fragmentation event compared to quark-fragmentation event. Thus

[*]Current address: Department of Physics, University of California, Berkeley, Berkeley, CA 94720-7300, USA

defined, an enhancement of 1.0 implies equal per-event production in gluon and quark fragmentation. In the photon-tagged analysis ($\Upsilon(1S) \to gg\gamma$ compared to $e^+e^- \to q\bar{q}\gamma$), we find almost no enhancement for protons ($\sim 1.2 \pm 0.1$), but a significant enhancement ($\sim 1.9 \pm 0.3$) for Λ's. This small measured proton enhancement rate is supported by a study of baryon production in $\chi_{b2} \to gg \to p + X$ relative to $\chi_{b1} \to q\bar{q}g \to p + X$. Overall, per-event baryon production in radiative two-gluon fragmentation is somewhat smaller than that observed in three-gluon decays of the $\Upsilon(1S)$. Our results for baryon production are inconsistent with the predictions of the JETSET (7.3) fragmentation model.

DOI: 10.1103/PhysRevD.76.012005 PACS numbers: 12.38.Aw, 12.38.Qk, 13.60.Hb, 13.87.Fh

I. INTRODUCTION

Understanding hadronization, the process by which elementary partons (gluons and quarks) evolve into mesons and baryons, is complicated by its intrinsically nonperturbative nature. Because of the fact that gluons carry two color indices whereas quarks carry only one, the intrinsic gluon-gluon coupling strength ($C_A = 3$) is larger than the intrinsic quark-gluon coupling strength ($C_F = 4/3$). Radiation of secondary and tertiary gluons is therefore expected to be more likely when hadronization is initiated by a gluon rather than by a quark. This results in a greater number of final-state hadrons as well as a larger average transverse momentum in the former case compared to the latter case. In the limit $Q^2 \to \infty$, the ratio of the number of hadrons produced in gluon-initiated jets to the number of hadrons produced in quark-initiated jets is expected, in lowest order, to approach a simple color-counting ratio 9/4 [1].

Many experiments studying e^+e^- collisions have searched for, and found, multiplicity and jet shape differences between quark and gluon fragmentation. At Z^0 energies, $q\bar{q}g$ events are distinguished by their three-jet topology. Within such events, quark and gluon jets can be separated by a variety of techniques including vertex tagging. Because gluons rarely fragment into heavy quarks, they will produce jets that form a vertex at the e^+e^- interaction point. Quark jets, to the contrary, tend to form a detached vertex when the jet contains a long-lived bottom or charm quark. For light-quark events with gluon radiation, however, the assignment of final-state hadrons to the initial state partons is generally more ambiguous and often relies on Monte Carlo simulations to determine the fraction of times that an observed hadron is correctly traced to a primary parton. At lower energies, one can exploit the decay characteristics of quarkonium states to directly compare gluon and quark fragmentation using data taken both on-resonance and off-resonance (on the continuum), respectively. The 10 GeV center-of-mass energy range offers a unique opportunity to probe quark and gluon-fragmentation effects, without relying on Monte Carlo simulation to associate the final-state hadrons with an initial state parton. CLEO [2] found that the thrust and charged multiplicity distributions of χ_{b0} and χ_{b2} two-gluon decays are more similar to $\Upsilon(1S) \to ggg$ than to continuum $e^+e^- \to q\bar{q}$ events; the reverse was found to be true for $\chi_{b1} \to q\bar{q}g$.

Specific particle production in gluon- and quark-fragmentation has also been studied. Within the limits of their precision, previous studies at SLD found inclusive production of pions, kaons, and protons to be equivalent for gluon-tagged and quark-tagged jets [3]. OPAL has measured inclusive charm production to be $(3.20 \pm 0.21 \pm 0.38)\%$ in gluon jets [4,5], more than an order of magnitude smaller than the rate observed in quark jets at the Z^0. ALEPH [6] and DELPHI [7] both measured inclusive bottom production in gluon-tagged jets to be $2\text{–}3 \times 10^{-3}$, again considerably smaller than that expected from charge counting in quark fragmentation. Most directly comparable to our current work, OPAL has also compared inclusive K^0_s and Λ production in gluon-tagged vs quark-tagged jets in $e^+e^- \to q\bar{q}g$ events, finding inclusive production ratios (g/q) consistent with unity ($0.94 \pm 0.07 \pm 0.07$ and $1.18 \pm 0.01 \pm 0.17$, respectively) [8].

The decay $\Upsilon(1S) \to gg\gamma$ allows one to directly compare the gg system in a $gg\gamma$ event with the $q\bar{q}$ system in $e^+e^- \to q\bar{q}\gamma$ events. In these cases, the system recoiling against the photon consists (to lowest order) of hadrons that have evolved from either a two-gluon or a quark-antiquark system. The properties of the recoil systems can then be compared.[1] Additionally, the radiative transitions from the radially excited Υ states to the orbitally excited χ_b triplet offer an opportunity to further probe fragmentation differences between decays of the $J = 0$ and $J = 2$ χ_b states, which decay predominantly to two gluons, vs decays of the $J = 1$ state. Since the $J = 1$ state is prohibited from decaying into two on-shell gluons, the decay into one hard and one soft, nearly on-shell virtual gluon (gg^*, followed by $g^* \to q\bar{q}$) is kinematically most favored. Statistical correlations between transition photons with inclusive production of particular final-state particles (X) allows a measurement of the relative yields of $gg \to X$:$q\bar{q}(g) \to X$ to these species.

[1]Although there may be gluon radiation from the initial partons, we do not distinguish such radiation explicitly in this analysis. Thus, the states that we are comparing are, strictly speaking, $gg\gamma$ and $q\bar{q}\gamma$ to lowest order only; additional gluon radiation, to which we are not experimentally sensitive, may be present in many of the events in our sample. Without the ability to adequately identify additional gluons, such higher-order radiative effects are therefore implicitly absorbed into the experimental measurement.

In an oversimplified "independent fragmentation" model, hadronization occurs independently for each parton. In such a picture, if fragmentation of each parton (gluon or quark) of a given energy is identical, then the ratio of particle production for $gg\gamma$:$q\bar{q}\gamma$:($\chi_b \to gg$):ggg hadronization should vary as: 2:2:2:3. In the opposite extreme, fragmentation occurs in the stretching "strings" between the two partons, in which case the above ratio should be 1:1:1:3.

In this analysis, we focus on the relative production rates of baryons (p and $\Lambda \to p\pi$) and heavy mesons ($\phi \to K^+K^-$ and $f_2(1270) \to \pi^+\pi^-$) in gluon vs quark fragmentation (charge conjugation is implied). A previous study noted enhancements in the production of ϕ, Λ, and p in three-gluon decays of the $\Upsilon(1S)$ [9], at a statistical significance of no more than 2–3 σ. That initial study also found approximately one unit larger charged multiplicity for three-gluon fragmentation of the $\Upsilon(1S)$ compared to $q\bar{q}$ fragmentation at a comparable center-of-mass energy. With the limited statistics available at that time, the additional unit of multiplicity could entirely be accounted for by enhanced three-gluonic production of baryons. We now have sufficient statistics to remeasure the three-gluon particle production rates, and also to compare, for the first time, inclusive production in two-gluon fragmentation vs inclusive production in three-gluon fragmentation.

Since the time of that initial study [9], other experimental data on quark/gluon-fragmentation differences in the $\sqrt{s} \sim 10$ GeV energy regime have recently become available, including:

(1) The observation that fragmentation of the $J = 1$ state of the χ_b triplet ($\chi_{b1} \to q\bar{q}g \to$ charm) results in charm production comparable to the underlying continuum; no such charm production is observed in the two-gluon decays of the $J = 0$ or $J = 2$ states [10].

(2) An enhancement in production of hidden charm in gluonic decays of the Υ resonances: $(\Upsilon(1S) \to ggg \to J/\psi + X)/(e^+e^- \to J/\psi + X) \gtrsim 5$ [11] at 90% C.L.

(3) Production of deuterons from resonant 3-gluon decays of both the $\Upsilon(1S)$ and $\Upsilon(2S)$ at the level of 10^{-3}; no significant production of deuterons is observed from the continuum [12]. Enhancements per event are ≥ 10.

(4) Production of η' in gluonic decays of the Υ resonance of similar magnitude to that observed in Υ decays via $q\bar{q}$: $(\Upsilon(1S) \to ggg \to \eta' + X)/(\Upsilon \to q\bar{q} \to \eta' + X) \sim 2/3$, integrated over momentum [13].

II. DETECTOR AND DATA SAMPLE

The CLEO-III detector [14–16] is a general purpose solenoidal magnet spectrometer and calorimeter. The main components of the detector used in this analysis are the drift chamber and the silicon detector used for track finding, the crystal calorimeter for energy measurements, and the Ring Imaging Cherenkov detector (RICH) and specific ionization loss in the drift chamber for particle identification. This system is very efficient ($\epsilon \geq 98\%$) for detecting tracks that have transverse momenta (p_T) relative to the beam axis greater than 200 MeV/c, and that are contained within the good fiducial volume of the drift chamber ($|\cos\theta| < 0.93$, with θ defined as the polar angle relative to the beam axis). Below this threshold, the charged particle detection efficiency in the fiducial volume decreases to approximately 90% at $p_T \sim 100$ MeV/c. For $p_T < 100$ MeV/c, the efficiency decreases roughly linearly to zero at a threshold of $p_T \approx 30$ MeV/c. Just within the solenoidal magnet coil is the electromagnetic calorimeter, consisting of 7800 thallium doped CsI crystals. The central region of the calorimeter covers about three-quarters of the solid angle and has an energy resolution of

$$\frac{\sigma_E}{E}(\%) = \frac{0.6}{E^{0.73}} + 1.14 - 0.01E, \quad (1)$$

with E the shower energy in GeV. This parametrization translates to an energy resolution of about 2% at 2 GeV and 1.2% at 5 GeV. Two end-cap regions of the crystal calorimeter extend solid angle coverage to about 95% of 4π, although the energy resolution is approximately 20%–60% worse, depending on energy. The tracking system, RICH particle identification system, and calorimeter are all contained within the 1.5 Tesla superconducting coil. Flux return and tracking chambers used for muon detection are located immediately outside the coil and in the two end-cap regions.

We use the CLEO-III data collected at the narrow Υ resonances as a source of ggg and $gg\gamma$ events, and data taken just below the narrow resonances, as well as the below-4S continuum ($\sqrt{s} = 10.55$ GeV) as a source of $q\bar{q}$ and $q\bar{q}\gamma$ events. Since $\Upsilon(4S) \to B\bar{B} \sim 100\%$, data collected on the broad $\Upsilon(4S)$ resonance is analyzed as a "control" sample, for which we expect no deviation from the below-4S continuum when we require a photon having $x_\gamma = p_\gamma/E_{\rm beam}$.

The γ in our continuum $q\bar{q}\gamma$ sample results primarily from initial state radiation (ISR) [17]. We compare events for which the fractional photon energies are the same, which ensures that the recoil systems (either two-gluon or $q\bar{q}$) have comparable energies. This convention deviates slightly from that of our previous publication [18] for which the scaling variable was the recoil mass of the gg and $q\bar{q}$ systems opposite the hard photon ($M_{\rm recoil}$, defined by $M_{\rm recoil} = \sqrt{4E_{\rm beam}^2(1 - E_\gamma/E_{\rm beam})}$). Comparison with continuum data taken ~20 MeV below each of the Υ resonances mitigates the effect of the ~1 GeV continuum center-of-mass energy extrapolation between the $\Upsilon(1S)$ and below-4S data samples required in the previous analysis [9], for which continuum data were only taken in the

10.55 GeV center-of-mass region. To compare ggg with $q\bar{q}$ hadronization, we simply bin by scaled momentum of the particle in question.

A. Event selection

We impose event-selection requirements identical to those used in our previous study of inclusive direct-photon production in Υ decays [19]. Those cuts are designed primarily to suppress backgrounds such as two-photon collisions, QED events (including tau pair production), and beam-gas and beam-wall collisions. Luminosity, event count, and photon yields ($z_\gamma > 0.5$) are given in Table I.

B. Background suppression

To determine the characteristics of resonant $\Upsilon \to gg\gamma$ events, we must subtract the background arising from nonresonant $q\bar{q}\gamma$ and $e^+e^- \to \tau\tau\gamma$ events produced in continuum e^+e^- annihilations at $\sqrt{s} = M_{\Upsilon(n\mathrm{S})}$, with $n = 1, 2$, or 3. This is done by direct scaling of the event samples collected off resonance on the nearby continuum.

In order to isolate continuum $q\bar{q}\gamma$ events, $\tau\tau\gamma$ contamination must be explicitly subtracted, using a Monte Carlo simulation of tau pair events. We find that $\tau\tau\gamma$ events comprise about 5% of the $q\bar{q}\gamma$ data sample passing the event-selection cuts [19]. Beam-gas and two-photon backgrounds were investigated and found to be negligibly small. The photon-tagged sample can also be contaminated by cases where the high-energy photon candidate is not produced directly, but is actually either a secondary daughter (mostly from π^0 decay) or a misidentified hadronic shower. Figure 1 illustrates the fraction of photons in Monte Carlo simulations of on-1S resonance and below-4S continuum, respectively, that are not produced in a direct decay.

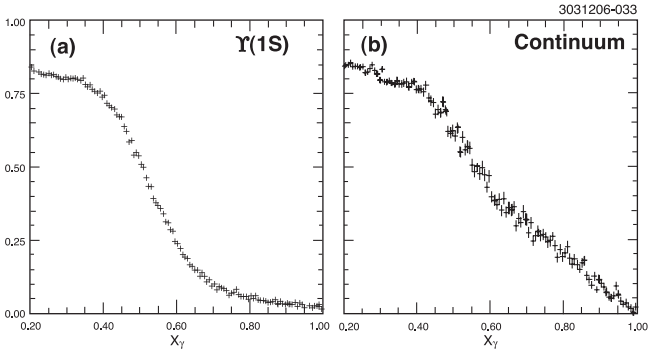

FIG. 1. JETSET Monte Carlo prediction for fraction of photons not produced directly, but through the decay of neutral particles (such as π^0, η, η', and ω) on the 1S resonance (left) and on the continuum below the 4S resonance (right).

Integrated over all tag photon momenta considered in this analysis, π^0 contamination comprises a $\sim$15% background to the direct-photon sample. Monte Carlo simulations also indicate that the π^0 contamination tends to cancel when we take ratios of resonant photon production to continuum photon production.

1. Particle identification

Our photon and particle identification procedures are identical to those developed in [19]. Photon candidates

TABLE I. Summary of data and JETSET Monte Carlo used in analysis. For each data set, we track the number of photons per unit luminosity, as well as the total number of observed hadronic events per unit luminosity $\mathcal{L}$. HadEvts denotes the total number of events in each sample identified as hadronic by our event-selection requirements. The number of photons having scaled momentum z_γ greater than 0.5 is presented in the last column. For $B\bar{B}$ Monte Carlo simulations, the small number of observed high-energy photons is a result of detector resolution and misreconstruction.

Data type	Type	Resonance	E_{cm} (GeV)	$\mathcal{L}$ (pb^{-1})	HadEvts ($\times 10^3$)	$N_\gamma(z > 0.5)$ ($\times 10^2$)
1S	Data	Υ(1S)	9.455–9.465	1220	22 780	2190
2S	Data	Υ(2S)	10.018–10.028	1070	9450	888
3S	Data	Υ(3S)	10.350–10.360	1420	8890	795
4S	Data	Υ(4S)	10.575–10.585	5520	18 970	1650
1S-CO	Data	$<\Upsilon$(1S)	9.400–9.454	144	515	57
2S-CO	Data	$<\Upsilon$(2S)	9.523–10.017	312	932	103
3S-CO	Data	$<\Upsilon$(3S)	10.083–10.349	185	532	59
4S-CO	Data	$<\Upsilon$(4S)	10.410–10.574	2100	5680	647
1S	JETSET MC	Υ(1S)	9.455–9.465		1160	99
2S	JETSET MC	Υ(2S)	10.018–10.028		9190	700
3S	JETSET MC	Υ(3S)	10.350–10.360		3890	270
4S	$B\bar{B}$ MC	Υ(4S)	10.575–10.585		8350	3
1S-CO	JETSET MC	$<\Upsilon$(1S)	9.400–9.454		8170	681
2S-CO	JETSET MC	$<\Upsilon$(2S)	9.523–10.017		7610	666
3S-CO	JETSET MC	$<\Upsilon$(3S)	10.083–10.349		12850	1150
4S-CO	JETSET MC	$<\Upsilon$(4S)	10.410–10.574		63630	5680

are selected from showers with widths and patterns of energy deposition consistent with those of a photon, as opposed to a neutral hadron (e.g., π^0 with overlapping photon showers, K_L^0, neutrons, etc.). To ensure that the events are well contained within the CLEO detector, we require $|\cos\theta_\gamma| < 0.707$ (θ_γ defined as before as the polar angle between the beam axis and the direct photon). For p (and $\bar{p}$), we require that charged tracks have specific ionizatation (dE/dx) and also RICH information consistent with those expected for protons. For momenta less than 1 GeV/c, we also require that the associated charged track dE/dx information be inconsistent (at the two standard-deviation level, with σ the momentum-dependent specific ionization resolution) with that expected for true pions. Although this results in a discontinuity in particle identification efficiency at 1 GeV/c, this requirement is necessary to ensure a high-purity sample. For all p and $\bar{p}$ candidates, we require that p ($\bar{p}$) momenta exceed 400 MeV/c to suppress beam-wall and fake backgrounds (i.e. K^+ and π^+ that pass p identification cuts) and also to eliminate concerns regarding protons ranging out in the beampipe. For reconstruction of ϕ ($f_2(1270)$) from kaons (pions) we require that pairs of oppositely charged tracks with momenta greater than 200 MeV/c (500 MeV/c) have particle identification information consistent with their assumed identities. Λ's are identified using the standard CLEO algorithms for reconstruction of detached vertices. Tables II and III summarize the raw, observed particle yields for our measurements, for data, and Monte Carlo simulations, respectively.

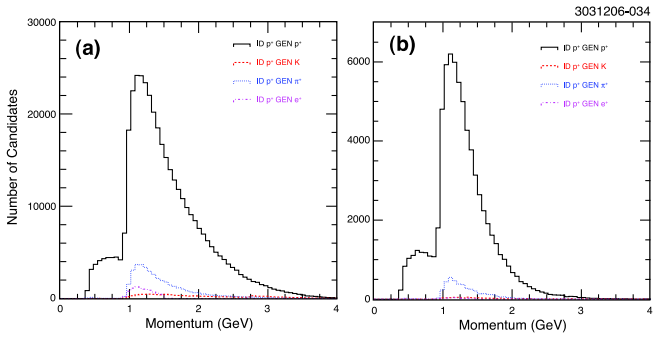

FIG. 2 (color online). (Left) Proton fakes for a sample of below-1S Monte Carlo simulations. The solid black curve shows the number of all particles identified as protons that were also tagged as true protons. The red dashed (blue dotted, magenta dash-dot) curve corresponds to those particles that were identified as protons, but that were actually kaons (pions, positrons). (Right) Same for on-1S event simulations. Note the discontinuity at 1 GeV/c, resulting from our momentum-dependent particle identification requirements below and above that momentum (see text).

2. Backgrounds to the proton sample

We use Monte Carlo simulations to assess fake proton backgrounds. Figure 2 illustrates proton fakes for a sample of below-1S Monte Carlo continuum simulations. The solid black curve shows the number of all particles identified as protons that were also tagged as true protons. The red dashed (blue dotted, magenta dash-dot) curve corresponds to those particles that were identified as protons, but that were generated as true kaons (pions, positrons) in the

TABLE II. Data particle yields for the on-1S resonance compared to continuum events. First column is particle type. Second and third columns show particle counts for the data in the format of (resonance yield)/(continuum yield) for the three-gluon analyses (2nd column) and two-gluon one-photon (3rd column) analyses.

Particle type	$(ggg)/(q\bar{q})$ [Data]	$(gg\gamma)/(q\bar{q}\gamma)$ [Data]
Λ	$(873\,600 \pm 1400)/(107\,300 \pm 600)$	$(3480 \pm 90)/(570 \pm 60)$
p	$(1\,399\,800 \pm 1200)/(295\,900 \pm 500)$	$(7970 \pm 90)/(2190 \pm 50)$
$\bar{p}$	$(1\,359\,500 \pm 1200)/(285\,400 \pm 500)$	$(7830 \pm 90)/(2090 \pm 50)$
ϕ	$(227\,900 \pm 1600)/(48\,300 \pm 800)$	$(1950 \pm 150)/(380 \pm 70)$
$f_2(1270)$	$(193\,000 \pm 4000)/(66\,500 \pm 1800)$	$(1600 \pm 400)/(400 \pm 200)$

TABLE III. Monte Carlo particle yields for the on-1S resonance compared to continuum events. First column is particle type. Second and third columns show particle counts for the data in the format of (resonance yield)/(continuum yield) for the three-gluon analyses (2nd column) and two-gluon one-photon (3rd column) analyses.

Particle type	$(ggg)/(q\bar{q})$ [JETSET MC]	$(gg\gamma)/(q\bar{q}\gamma)$ [JETSET MC]
Λ	$(136\,700 \pm 500)/(1\,333\,200 \pm 2000)$	$(690 \pm 30)/(6410 \pm 150)$
p	$(266\,600 \pm 500)/(3\,334\,200 \pm 1800)$	$(1650 \pm 40)/(20\,660 \pm 140)$
$\bar{p}$	$(257\,300 \pm 500)/(3\,198\,300 \pm 1800)$	$(1590 \pm 40)/(19\,880 \pm 140)$
ϕ	$(48\,100 \pm 900)/(837\,000 \pm 4000)$	$(380 \pm 80)/(6000 \pm 800)$

Monte Carlo simulated event sample. Proton backgrounds are observed to be present at the ~10% level and are expected to largely cancel in the enhancement ratio.

C. Signal definition

In this analysis we measure particle enhancements in both the ggg and $gg\gamma$ decays of the upsilon system, relative to $q\bar{q}(\gamma)$ production on the underlying continuum. Our definition of enhancement is given quantitatively as the continuum-subtracted resonance yield relative to the continuum yield. Thus defined, an enhancement of 1 indicates that a given particle is produced as often (per event) on the continuum as on the resonance. Note that our definition of "continuum" here includes both continuum below the resonance peak, as well as resonance $\rightarrow q\bar{q}$ through vacuum polarization; i.e., all $e^+e^- \rightarrow q\bar{q}$-like processes which must be explicitly subtracted in determining the characteristics of 3-gluon resonant decays.[2] Furthermore, note that for the $\Upsilon(2S)$ and $\Upsilon(3S)$ data, there is no subtraction of cascades to lower Υ states or χ_b decays. In what follows, "$\Upsilon(2S)$" denotes a sum over $\Upsilon(2S)$ direct, $\Upsilon(2S) \rightarrow \Upsilon(1S) + X$, and $\Upsilon(2S) \rightarrow \gamma\chi_b$. Assuming the direct decays of the Υ resonances are identical, an $\Upsilon(2S)$ enhancement smaller than that of the $\Upsilon(1S)$ implies that the enhancements from the first and third processes enumerated above are therefore smaller than for the $\Upsilon(1S)$.

In general we have two continuum-subtraction options: we may determine enhancements for all resonances relative to the below-4S continuum (for which the statistics are largest, but the difference in e^+e^- collision energies is also largest) or we may find enhancements relative to their individual below-resonant continua. For mass-fitted particles we normalize exclusively to the below-4S continuum, as the individual continua (below-1S, -2S, and -3S) have insufficient statistics to yield well-fitted mass peaks. For particle counts determined by the momentum spectra (protons and antiprotons), we normalize to both the below-4S continuum as well as the resonance-specific continua and incorporate the differences in the enhancements calculated in the two cases into the overall systematic error.

D. Particle production in three-gluon vs $q\bar{q}$ events

The previous CLEO-I [9] analysis already observed significant enhancements of p and Λ produced in 3-gluon decays of the 1S relative to the below-4S continuum. We repeat that analysis with our larger, current data set, as detailed below. Errors on particle yields are obtained from the error returned from the fit if the particle count is obtained by fitting a mass peak (Λ, ϕ, f_2), or by the square root of the total count if the particle count is obtained from a simple integration over the momentum spectrum (p, $\bar{p}$). For the ggg analysis described below, we determine enhancements as a function of scaled momentum and also calculate momentum-integrated enhancements for each particle, to allow comparison with previous results.

E. $gg\gamma$ analysis

For the $gg\gamma$ analysis we normalize the total particle yield to the photon count in a given photon momentum bin. For each bin, we then find the fractional contamination $\mathcal{F}$ of resonance photons "R" due to the underlying continuum "C" (Eq. (2)) in terms of the visible cross section σ for high-energy photons and the known beam energies "E"

$$\mathcal{F} = \frac{\sigma^C_{z_\gamma>0.5}}{\sigma^R_{z_\gamma>0.5}}\left(\frac{E^C}{E^R}\right)^2. \quad (2)$$

Once $\mathcal{F}$ is known, the resonance yield can be extracted by straightforward algebra.

III. RESULTS FROM UPSILON DECAYS

A. ggg enhancements with respect to $q\bar{q}$

1. Baryon enhancements

Figure 3 presents our Λ enhancements binned according to scaled momentum, defined as before as the momentum

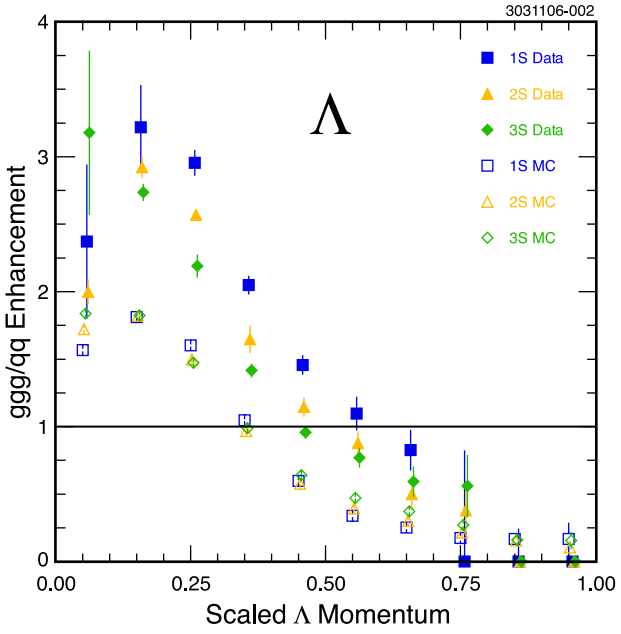

FIG. 3 (color online). Raw (i.e., observed, and with no relative efficiency corrections applied) enhancements for $ggg \rightarrow \Lambda + X$ binned according to scaled momentum ($p_\Lambda/E_{\text{beam}}$). Blue square (gold triangle, green diamond) symbols correspond to enhancements on the 1S (2S, 3S) resonance. Closed symbols are data, open symbols are derived from JETSET 7.3 Monte Carlo simulations. No relative efficiency corrections have been applied to these "raw" data.

[2]Vacuum-polarization processes are subtracted by direct scaling of the continuum using the $\Upsilon \rightarrow \gamma^\star \rightarrow q\bar{q}$ values tabulated previously [19].

of the particle divided by the beam energy. In the figure, blue square (gold triangle, green diamond) symbols correspond to enhancements on the 1S (2S, 3S) resonance. Closed symbols are data and open symbols are JETSET 7.3 [20] event generator simulations followed by the full CLEO-III GEANT-based [21] Monte Carlo detector simulation. From the figure we see that the Υ's show qualitatively the same behavior for all resonances (1S, 2S, 3S) in both data and Monte Carlo, namely, a smooth decrease in enhancement with increasing scaled momentum. We note that the enhancements decrease steadily as one goes from $\Upsilon(1S)$ to $\Upsilon(2S)$ to $\Upsilon(3S)$ and that the data, at all scaled momenta, show significantly greater enhancements than do the Monte Carlo simulations.

Figure 4 shows the p and $\bar{p}$ enhancements. With the exception of the very lowest momentum bin, which is most subject to range-out effects, the consistency between the two indicates that beam-wall and beam-gas backgrounds (which produce an excess of p in the beam) are not substantial. As compared to Λ enhancements, p and $\bar{p}$ enhancements are lower and the differences between 1S, 2S, and 3S enhancements (as well as the differences between data and Monte Carlo) are smaller.

2. ϕ and $f_2(1270)$ enhancements

Figure 5 shows ϕ enhancement results binned according to scaled momentum. Symbols are as above with blue square (gold triangle, green diamond) corresponding to enhancements on the 1S (2S, 3S) resonance. Closed symbols are data and open symbols are JETSET Monte Carlo. Here, we have normalized the resonant production at 9.46 GeV to the continuum production at 10.55 GeV. For ϕ production, the lowest momentum bins for the resonance are particularly sensitive to low-momentum kaon acceptance. Figure 5 also shows the f_2 enhancement results binned according to scaled momentum. The f_2 peak is not well defined at low momentum (lowest two bins). No Monte Carlo comparison is presented since our current

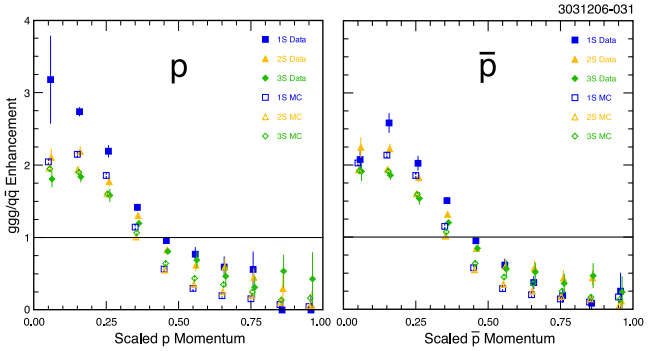

FIG. 4 (color online). (Left) Raw enhancements for $ggg \to p + X$ binned according to scaled momentum. Blue square (gold triangle, green diamond) symbols correspond to enhancements on the 1S (2S, 3S) resonance. Closed symbols are data, open symbols are JETSET Monte Carlo. (Right) Same for $\bar{p}$.

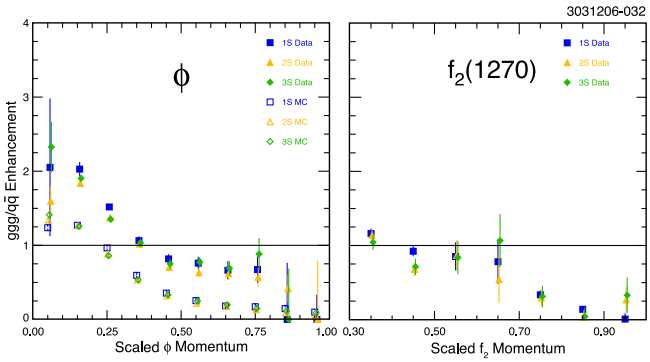

FIG. 5 (color online). (Left) Raw enhancements for ggg ϕ binned according to scaled momentum. Blue square (gold triangle, green diamond) symbols correspond to enhancements on the 1S (2S, 3S) resonance. Closed symbols are data, open symbols are JETSET Monte Carlo. (Right) Enhancements for $f_2(1270)$.

Monte Carlo event generator, by default, will not generate f_2 tensor particles.

3. Particle momentum-integrated enhancements

Figure 6 shows the particle enhancements integrated over all momenta for each particle (summarized numeri-

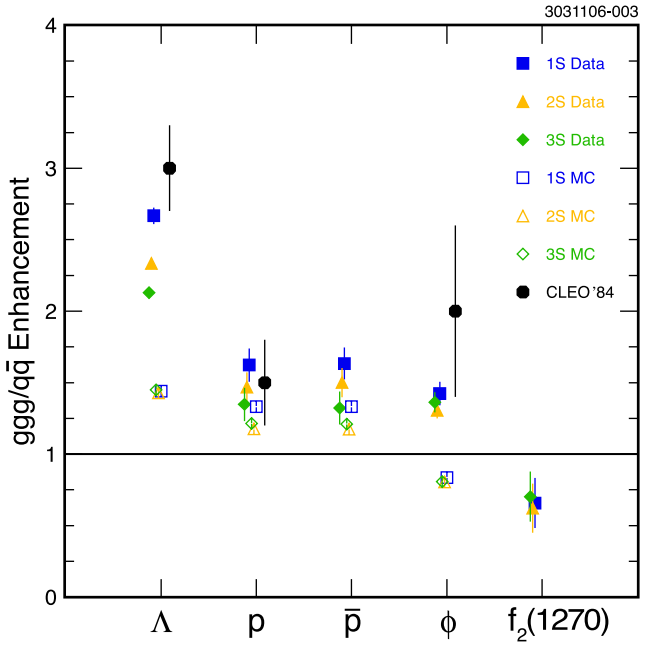

FIG. 6 (color online). Compilation of momentum-integrated enhancements for ggg events. Blue square (gold triangle, green diamond) symbols correspond to enhancements on the 1S (2S, 3S) resonance. Closed symbols are data, open symbols are JETSET Monte Carlo. Systematic errors and relative efficiencies have now been included for this compilation. The CLEO84 study did not measure an enhancement for $f_2(1270)$ and also only presented a single enhancement for the sum of p and $\bar{p}$.

cally in Table V). We note that the baryons (Λ, p, $\bar{p}$) have enhancements greater than 1, the ϕ meson enhancement is closer to unity, and the production of the tensor f_2 is less than unity over our kinematic acceptance region. Our results are, in general, numerically consistent with the prior CLEO-I analysis, albeit with considerably improved statistical precision.

B. $gg\gamma$ enhancements with respect to $q\bar{q}\gamma$

There are sufficient CLEO-III statistics to present enhancements binned according to photon momentum, but integrated over particle momenta for Λ, p, and $\bar{p}$. For all particles, we also present momentum-integrated enhancements.

1. Baryon enhancements

Figure 7 shows Λ results binned according to scaled photon momentum. For Λ's, as compared to the momentum-integrated $ggg/q\bar{q}$ enhancements, we observe a lower overall enhancement, on the order of 2 as opposed to 2.5–3 for the Υ's (Fig. 6). Figure 8 shows p and $\bar{p}$ enhancement results binned according to scaled photon momentum. We note that $gg\gamma/q\bar{q}\gamma$ p and $\bar{p}$ exhibit enhancements similar to that of Λ's.

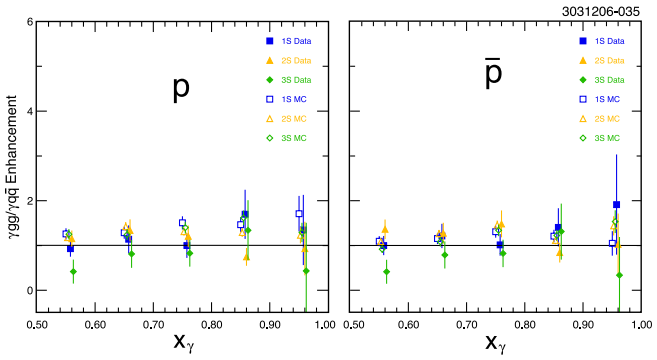

FIG. 8 (color online). (Left) Raw enhancements for $gg\gamma \to p + X$ binned according to scaled photon energy, integrated over all p momenta. Blue square (gold triangle, green diamond) symbols correspond to enhancements on the 1S (2S, 3S) resonance. Closed symbols are data, open symbols are JETSET Monte Carlo. (Right) Same for $\bar{p}$.

2. Photon momentum-integrated enhancements

Figure 9 shows the photon momentum-integrated enhancements for each particle (summarized numerically in Table V). We note that all baryons show enhancements lower than in the 3-gluon case (Fig. 6).

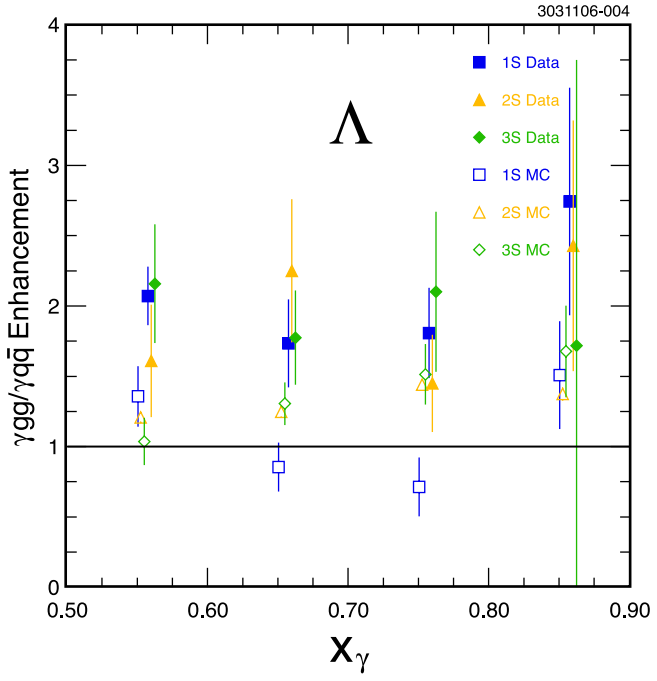

FIG. 7 (color online). Raw enhancements for $gg\gamma \to \Lambda + X$ binned according to scaled photon energy, integrated over all Λ momenta. Blue square (gold triangle, green diamond) symbols correspond to enhancements on the 1S (2S, 3S) resonance. Closed symbols are data, open symbols are JETSET Monte Carlo.

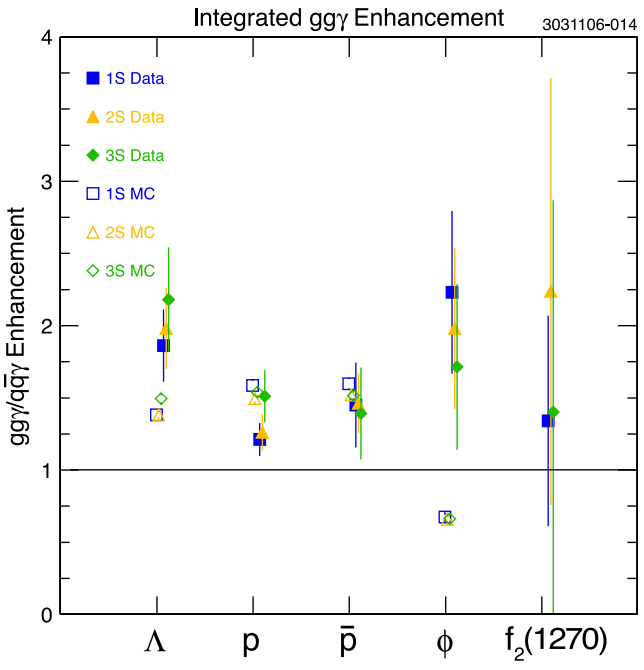

FIG. 9 (color online). Compilation of photon momentum-integrated enhancements for $gg\gamma$ events. Blue square (gold triangle, green diamond) symbols correspond to enhancements on the 1S (2S, 3S) resonance. Closed symbols are data, open symbols are JETSET Monte Carlo. Systematic errors and relative efficiencies have now been included for this compilation.

IV. INCLUSIVE PROTON PRODUCTION IN χ_{bJ} DECAYS

Photon transitions of the $\Upsilon(2S)$ and $\Upsilon(3S)$ to the $\chi_b(')$ states allow us to measure the baryon yields in $\chi_b(')$ decay, in association with a radiative transition photon "tag." Typical photon tag energies in this case are of order 80–160 MeV. Because of the large $\pi^0 \to \gamma\gamma$ backgrounds to such transition photons at these relatively low photon energies, which compromise the statistical power of such tags, the data permit only an extraction of the proton and antiproton enhancements. Of particular interest is the proton yield in χ_{b2} vs χ_{b1} decays; the former is expected to be dominated by decays via two gluons, the latter is expected to be dominated by decays to $q\bar{q}(g)$, with the gluon expected to carry away very little momentum.

To ensure that photon-finding systematics largely cancel in the ratio, and to also exclude possible contributions from initial state radiation, we compare particle yields within the χ_{bJ} system directly rather than normalizing, e.g. relative to the underlying $e^+e^- \to q\bar{q}(\gamma)$ continuum. We first conduct a Monte Carlo study to determine the relative efficiency of reconstructing a $J = 2$ transition photon relative to $J = 1$ event, and also the efficiency when we require that a proton be found in addition to the transition photon. We compile statistics on the $\chi_b(') \to p(\bar{p}) + X$ analyses, separately for $J = 0/J = 1$ and for $J = 2/J = 1$. For the latter, the overlap of the two observed photon signals results in a highly correlated event yield for the two transitions. We correspondingly extract this ratio from a signal fit to a double Gaussian plus a smooth background. For the former, we simply fit two separate signal Gaussians directly. We find that the efficiency for reconstructing photon-proton correlations in $\chi_{b2} \to gg$ decays is approximately 95% that for photon-proton correlations in $\chi_{b1} \to q\bar{q}(g)$ events.

To check the sensitivity to our particle identification criteria, we have compared results using very tight proton identification requirements (with a reduction in efficiency by more than 50%) vs the "standard" loose proton identification criteria used above. We obtain a comparable correction factor for the $J = 2/J = 1$ event yields using more restrictive particle identification criteria.

Results are presented in Table IV. We note that the observed enhancements are, again, smaller than those observed in comparing three-gluon fragmentation from the Υ resonance with $q\bar{q}$ fragmentation.

V. CROSS-CHECKS AND SYSTEMATICS

In order to verify our procedures and probe possible systematic uncertainties, two primary cross-checks were employed. We first compare the Monte Carlo enhancements at the event generator-level with those determined after the generated events are processed through the full CLEO-III detector simulation ("detector-level"), as a

TABLE IV. Summary of inclusive proton (and antiproton) results for χ_{bJ} decays. For checks of internal consistency, data have been separated into subsamples, labeled with capital roman letters. For $J = 2$ relative to $J = 1$, e.g., the scale of systematic uncertainties is set by the constancy of the value across subsamples collected in different running periods (r.m.s. ~ 0.03), the magnitude of relative efficiency corrections (~ 0.05), and the consistency of results obtained using different particle identification criteria. For summed results (labeled "all"), the second error shown is the systematic error.

Data set	Particle ID	$(\frac{\chi_{b2}\to pX}{\chi_{b1}\to pX})$	$(\frac{\chi_{b0}\to pX}{\chi_{b1}\to pX})$
(3S A)	loose	1.116 ± 0.017	1.19 ± 0.046
(3S B)	loose	1.080 ± 0.016	1.00 ± 0.034
(3S C)	loose	1.086 ± 0.011	1.054 ± 0.047
(3S D)	tight	1.103 ± 0.027	1.091 ± 0.097
3S, all		$1.109 \pm 0.007 \pm 0.040$	$1.082 \pm 0.025 \pm 0.060$
(2S A)	tight	1.066 ± 0.028	1.03 ± 0.13
(2S B)	loose	1.075 ± 0.018	1.36 ± 0.15
(2S C)	loose	1.076 ± 0.017	0.99 ± 0.11
(2S D)	loose	1.065 ± 0.015	1.06 ± 0.11
(2S B)	tight	1.076 ± 0.047	1.39 ± 0.28
(2S C)	tight	1.039 ± 0.040	1.17 ± 0.22
(2S D)	tight	1.024 ± 0.035	0.88 ± 0.20
2S, all		$1.068 \pm 0.010 \pm 0.040$	$1.11 \pm 0.15 \pm 0.20$
Monte Carlo (3S A)	loose	1.057 ± 0.016	1.030 ± 0.072
Monte Carlo (3S A)	tight	1.034 ± 0.015	1.042 ± 0.066
Monte Carlo (3S B)	tight	1.041 ± 0.013	1.051 ± 0.049
MC, 3S all sets		1.043 ± 0.008	1.043 ± 0.036
Monte Carlo (2S A)	tight	1.052 ± 0.014	1.121 ± 0.058
Monte Carlo (2S A)	loose	1.043 ± 0.015	1.076 ± 0.061
MC, 2S all sets		1.046 ± 0.010	1.061 ± 0.025

function of momentum. In general, these enhancements will differ for several reasons, including differences in: (a) the efficiencies for finding recoil particles in $q\bar{q}\gamma$ vs $gg\gamma$ events resulting from angular distribution, event multiplicity, and particle momentum differences, (b) event-selection efficiencies, (c) π^0 contamination levels, and (d) recoil center-of-mass discrepancies between the continuum data under the $\Upsilon(1S)$ resonance vs the below-$\Upsilon(4S)$ continuum. In cases where the generator-level and detector-level enhancements are statistically inconsistent with each other at the 2σ level, we use the ratio between the generator-level and detector-level enhancements as a correction factor and take half of the amount by which this correction deviates from unity as an estimated systematic error. Typical corrections are of order $\leq 10\%$. (Note that these corrections have already been incorporated into the results presented in Figures 6 and 9). Figures 10 and 11 show the comparison of p enhancements determined at the event-generator vs post-detector-simulation levels of Monte Carlo simulation.

In addition to the comparison of generator vs detector-level enhancements, we have made an additional (largely redundant) check of possible biases due to nondirect photons resulting from, e.g., $\pi^0 \to \gamma\gamma$, $\eta \to \gamma\gamma$, etc. Using Monte Carlo simulations, we compare the enhancements obtained using direct photons only, compared with the enhancements obtained when we include all Monte Carlo photons which pass our photon selection, independent of parentage. Integrated over momentum, this again constitutes a $\sim$5% effect, and is conservatively included as an additional (in quadrature) systematic error.

To test the sensitivity of our analysis procedures across different running periods, we have calculated the enhancements for photon-tagged $\Upsilon(4S)$ on-resonance events vs photon-tagged below-$\Upsilon(4S)$ continuum events, spanning the full CLEO-III data set. Since $\Upsilon(4S) \to B\bar{B} \sim 100\%$, we expect that any event having a photon with $z_\gamma > 0.5$ is a continuum event. Hence, the calculated enhancement should be zero. In all cases, save for $\bar{p}$, we find good agreement between the below-4S continuum particle yields per photon tag, and the on-4S particle yields per photon tag. For $\bar{p}$, we find deviations from the null expectation at the level of $\approx$ 5%–7%, and incorporate these deviations (bin by bin in momentum) into our total systematic error for that particular case. For the case of the broad f_2 resonance, sensitivity to our parametrization of the smooth background also contributes a non-negligible systematic uncertainty.

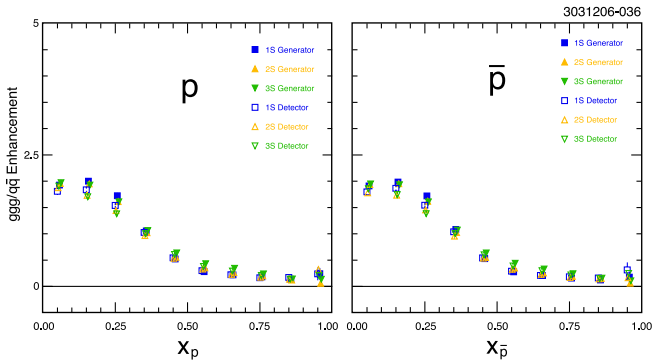

FIG. 10 (color online). (Left) Scaled momentum binned enhancements for $ggg \to p + X$ at generator level and after detector simulation. Blue square (gold triangle, green inverted triangle) symbols correspond to enhancements on the 1S (2S, 3S) resonance. Closed (open) symbols are generator (detector) level Monte Carlo enhancements. (Right) Same for $\bar{p}$.

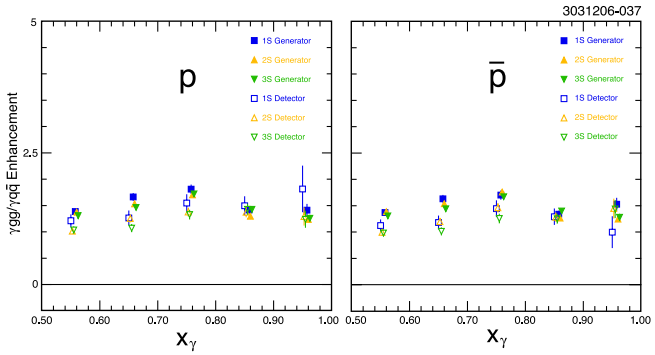

FIG. 11 (color online). (Left) Scaled momentum binned enhancements for $gg\gamma$ decays to p at generator level and after detector simulation. Blue square (gold triangle, green inverted triangle) symbols correspond to enhancements on the 1S (2S, 3S) resonance. Closed (open) symbols are generator (detector) level Monte Carlo enhancements. (Right) Same for $\bar{p}$.

We note that most systematic errors cancel in our ratios. The largest nonzero components are the efficiency bias ($\sim$ 10%), as measured by the deviation between the generator-level and detector-level enhancements, the nondirect-photon background ($\sim$ 5%), and the run dependence of our result, as measured by our expectation that the photon-tagged on-4S data should yield identical enhancements as for the below-4S continuum data ($\sim$ 6%), all added in quadrature. Our results with statistical and systematic errors are listed in Table V. The statistical uncertainties in the data are typically of order 10%, with the exception of $gg\gamma/q\bar{q}\gamma$ for ϕ and f_2, which are of poorer statistical quality.

VI. DISCUSSION AND SUMMARY

We have, for the first time, measured the momentum-dependent ratio of baryon and meson production in gluon vs quark fragmentation at $\sqrt{s} \sim 10$ GeV. After reproducing the previously measured per-event baryon production rates in three-gluon decays of the $\Upsilon(1S)$ resonance relative to the underlying continuum, we have extended that study to include the other narrow Υ resonances and, with higher statistics, now explicitly examine the momentum dependence of the enhancements for all these states. Integrated over momentum, we observe approximately 5% (10%)

TABLE V. Numerical summary of momentum-integrated enhancement results. Second and third columns show results from Fig. 9, the photon momentum-integrated $gg\gamma/q\bar{q}\gamma$ study. Fourth and fifth columns show results from Fig. 6, the particle momentum-integrated $ggg/q\bar{q}$ study. MC refers to JETSET Monte Carlo. Data errors are statistical and systematic; MC errors are purely statistical. For the f_2, we present 90% C.L. upper limits, given the poor statistical significance of the $gg\gamma/q\bar{q}\gamma$ enhancements.

Particle	$gg\gamma/q\bar{q}\gamma$ data	$gg\gamma/q\bar{q}\gamma$ MC	$ggg/q\bar{q}$ data	$ggg/q\bar{q}$ MC
Λ (1S)	$1.86 \pm 0.25 \pm 0.03$	1.38 ± 0.039	$2.668 \pm 0.027 \pm 0.051$	1.440 ± 0.003
Λ (2S)	$1.98 \pm 0.27 \pm 0.08$	1.38 ± 0.018	$2.333 \pm 0.019 \pm 0.021$	1.428 ± 0.002
Λ (3S)	$2.18 \pm 0.36 \pm 0.02$	1.49 ± 0.023	$2.128 \pm 0.021 \pm 0.010$	1.450 ± 0.002
p (1S)	$1.21 \pm 0.11 \pm 0.03$	1.582 ± 0.034	$1.623 \pm 0.014 \pm 0.116$	1.331 ± 0.005
p (2S)	$1.26 \pm 0.11 \pm 0.06$	1.495 ± 0.018	$1.469 \pm 0.011 \pm 0.103$	1.177 ± 0.003
p (3S)	$1.51 \pm 0.17 \pm 0.06$	1.53 ± 0.021	$1.348 \pm 0.013 \pm 0.116$	1.214 ± 0.003
$\bar{p}$ (1S)	$1.45 \pm 0.14 \pm 0.26$	1.589 ± 0.034	$1.634 \pm 0.014 \pm 0.111$	1.333 ± 0.005
$\bar{p}$ (2S)	$1.46 \pm 0.12 \pm 0.17$	1.513 ± 0.018	$1.500 \pm 0.011 \pm 0.102$	1.175 ± 0.003
$\bar{p}$ (3S)	$1.39 \pm 0.17 \pm 0.27$	1.51 ± 0.020	$1.323 \pm 0.013 \pm 0.115$	1.210 ± 0.003
ϕ (1S)	$1.78 \pm 0.49 \pm 0.08$	0.673 ± 0.013	$1.423 \pm 0.051 \pm 0.065$	0.836 ± 0.003
ϕ (2S)	$1.73 \pm 0.52 \pm 0.06$	0.658 ± 0.012	$1.308 \pm 0.041 \pm 0.041$	0.805 ± 0.001
ϕ (3S)	$1.87 \pm 0.81 \pm 0.06$	0.662 ± 0.015	$1.355 \pm 0.054 \pm 0.047$	0.808 ± 0.002
$f_2(1270)$ (1S)	$1.34 \pm 0.84 \pm 0.15$ (< 2.74)	—	$0.658 \pm 0.058 \pm 0.175$	—
$f_2(1270)$ (2S)	$2.22 \pm 1.53 \pm 0.20$ (< 4.68)	—	$0.621 \pm 0.094 \pm 0.171$	—
$f_2(1270)$ (3S)	$1.41 \pm 1.48 \pm 0.10$ (< 3.87)	—	$0.702 \pm 0.104 \pm 0.175$	—

lower baryon production per event for $\Upsilon(2S)$ ($\Upsilon(3S)$) decays compared to the vector ground state. Nevertheless, the per-event production of Λ's for each of the narrow Υ resonances is observed to be greater than twice that of continuum fragmentation at the same center-of-mass energy.

We additionally compare, for the first time, particle production in two-gluon vs quark-antiquark fragmentation. We find, in particular, that baryon production (per event) in two-gluon decays is somewhat smaller ($\sim 20\%$ for baryons) than that observed in three-gluon decays. For Λ production, we still observe a significant ($\sim \times 2$) enhancement in two-gluon fragmentation relative to quark-antiquark fragmentation, although the excess enhancement for p is $\leq 10\%$. For p, which represent our highest-statistics sample, our results are inconsistent with a model where baryon production in gluon fragmentation is only a function of the available center-of-mass energy; clearly, the number of fragmenting partons is also important, although our measured enhancements fall short of the expectations from a naive independent fragmentation model. Our results, for all measured integrated enhancements are presented in Table V.

Although event generators such as JETSET have had tremendous success in describing the gross details of particle production in e^+e^- collisions, our study indicates that there may still be considerable tuning needed at the single-particle yield level.

ACKNOWLEDGMENTS

We gratefully acknowledge the effort of the CESR staff in providing us with excellent luminosity and running conditions. D. Cronin-Hennessy and A. Ryd thank the A. P. Sloan Foundation. This work was supported by the National Science Foundation, the U.S. Department of Energy, and the Natural Sciences and Engineering Research Council of Canada.

[1] S. J. Brodsky and J. Gunion, Phys. Rev. Lett. **37**, 402 (1976); K. Konishi, A. Ukawa, and G. Veneziano, Phys. Lett. B **78**, 243 (1978).
[2] S. Alam *et al.* (CLEO Collaboration), Phys. Rev. D **46**, 4822 (1992).
[3] H. Kang *et al.* (SLD Collaboration), Int. J. Mod. Phys. A **16S1A**, 226 (2001).
[4] G. Abbiendi *et al.* (OPAL Collaboration), Eur. Phys. J. C **37**, 25 (2004).
[5] G. Abbiendi *et al.* (OPAL Collaboration), Eur. Phys. J. C **13**, 1 (2000).
[6] R. Barate *et al.* (ALEPH Collaboration), Phys. Lett. B **434**, 437 (1998).
[7] P. Abreu *et al.* (DELPHI Collaboration), Phys. Lett. B **405**, 202 (1997).
[8] K. Ackerstaff *et al.* (OPAL Collaboration), Eur. Phys. J. C **8**, 241 (1999).
[9] S. Behrends *et al.* (CLEO Collaboration), Phys. Rev. D **31**, 2161 (1985).
[10] D. Besson (CLEO Collaboration), *The International Conference on High Energy Physics, Moscow, Russia, 2006* (unpublished).

[11] R. A. Briere *et al.* (CLEO Collaboration), Phys. Rev. D **70**, 072001 (2004).
[12] D. M. Asner *et al.* (CLEO Collaboration), Phys. Rev. D **75**, 012009 (2007).
[13] O. Aquines *et al.* (CLEO Collaboration), Phys. Rev. D **74**, 092006 (2006).
[14] G. Viehhauser *et al.*, Nucl. Instrum. Methods Phys. Res., Sect. A **462**, 146 (2001).
[15] D. Peterson *et al.*, Nucl. Instrum. Methods Phys. Res., Sect. A **478**, 142 (2002).
[16] M. Artuso *et al.*, Nucl. Instrum. Methods Phys. Res., Sect. A **554**, 147 (2005).
[17] F. A. Berends and R. Kleiss, Nucl. Phys. **B178**, 141 (1981).
[18] M. S. Alam *et al.* (CLEO Collaboration), Phys. Rev. D **56**, 17 (1997).
[19] D. Besson *et al.* (CLEO Collaboration), Phys. Rev. D **74**, 012003 (2006).
[20] T. Sjostrand, Report No. CERN-TH/7111-93.
[21] R. Brun *et al.*, GEANT v. 3.14, CERN Report No. CERN CC/EE/84-1, 1987.